5

X-ray Binaries

https://doi.org/10.1017/S0074180900055753 Published online by Cambridge University Press

HIGH-MASS X-RAY BINARIES: RECENT DEVELOPMENTS

F. NAGASE

The Institute of Space and Astronautical Science
3-1-1 Yoshinodai, Sagamihara, Kanagawa 229, Japan

1. Introduction

There are about a dozen extensively investigated high-mass X-ray binaries (HMXBs), including LMC X-4, Cen X-3, 4U 1700–37, SMC X-1, Cyg X-1, and Vela X-1. Bhattacharya & Van den Heuvel (1991) compiled a list of "standard" HMXBs (see table 8 of their review article) and most of them, except for Cyg X-1 and 4U 1700–37, are accreting X-ray pulsars with an early-type or a Be star companion. Cyg X-3 was long considered to be a low-mass X-ray binary (LMXB). It was, however, recently revealed from infrared observations that the companion star has characteristics of a Wolf-Rayet star and it may be a fairly massive helium star (Van Kerkwijk *et al.* 1992; Van Kerkwijk 1993). I shall review here some recent progress in observational studies of the "standard" HMXBs and Cyg X-3.

I will concentrate on two topics and review mainly observational results from GINGA and ASCA. The first topic is a brief summary of measurements of the orbital period changes in X-ray binary pulsars. A few results have been added recently from GINGA observations, in addition to the well established results on the orbital period decay in the Cen X-3 binary system (Murakami *et al.* 1983; Kelley *et al.* 1983). The orbital period changes of LMXBs will be briefly compared with those of HMXBs. The second topic deals with results obtained from recent high-resolution spectroscopic observations with the ASCA SIS detectors (CCD cameras). Since the spectra obtained with ASCA from black-hole candidates, LMXBs and the jet-like object SS 433 are reviewed in these proceedings by Inoue, I here present results obtained for X-ray pulsars and Cyg X-3, and discuss line emission from plasmas in photo-ionization equilibrium.

J. van Paradijs et al., (eds.), Compact Stars in Binaries, 289–300.

2. Measurements of Orbital Period Change

Studies of orbital period changes in HMXBs provide insight into their present state, e.g. the presence of tidal torques and the rotation rate of the optical counterparts, and their evolution, including their lifetime as bright X-ray sources as the Roche lobe moves through the stellar atmosphere. Before GINGA observations, Cen X-3 was the only X-ray binary pulsar for which a finite rate of orbital period change had been measured (Murakami *et al.* 1983; Kelley *et al.* 1983).

GINGA observations between 1987 and 1992 extended the observational baseline for several X-ray pulsars, with maximum intervals of nearly 20 years between UHURU and GINGA. This extension of the baseline enables us to examine in detail the rate of change of the orbital periods which in the case of X-ray pulsars can be supplemented by accurate determinations of the orbital parameters through fitting of the Doppler shifted pulse arrival times. In the case of Cyg X-3 the orbital period ($P_{\rm orb}$) and its change rate ($\dot{P}_{\rm orb}$) are derived from the modulation of the X-ray light curve. However, accurate measurements of the $P_{\rm orb}$ and $\dot{P}_{\rm orb}$ are possible in Cyg X-3 because of the long baseline of observations, stable modulation of the X-ray light curve and the extremely short (0.2 d) binary period.

A negative rate of period change $\dot{P}_{\rm orb}/P_{\rm orb} = (-1.78 \pm 0.08)\ 10^{-6}\,{\rm yr}^{-1}$ was first obtained for Cen X-3 using the eclipse data obtained with UHURU, SAS-3 and HAKUCHO (Kelley *et al.* 1983). The orbital decay was confirmed by Nagase *et al.* (1992) by adding the TENMA and GINGA determinations of mid-eclipse time using the orbital Doppler analysis of pulse arrival times; the rate of change was improved to $\dot{P}_{\rm orb}/P_{\rm orb} = (-1.738 \pm 0.004)\ 10^{-6}\,{\rm yr}^{-1}$(see Fig. 1). It is worth pointing out that there are significant deviations of the residuals from the best-fit ephemeris in the early UHURU data. This is unlikely to be intrinsic to the nature of the binary evolution, and Deeter (private communication) suggests from his reexamination of the UHURU data that they can possibly be fit consistently to the currently improved orbital parameters.

Although Her X-1 is a LMXB, precise determination of the orbital parameters is possible for this X-ray pulsar, utilizing pulse arrival time analysis to the orbital Doppler effect. It was found by Deeter *et al.* (1991) that the mid-eclipse epoch of Her X-1 determined from the GINGA data occurs about 40 s earlier than expected from the extrapolation of the previously determined ephemeris. By combining the GINGA ephemeris of Her X-1 with that of previous measurements, they obtained a finite rate of orbital period decrease of $\dot{P}_{\rm orb}/P_{\rm orb} = (-1.32 \pm 0.16)\ 10^{-8}\,{\rm yr}^{-1}$. This value is about two order of magnitude smaller than that for Cen X-3 and is the smallest finite value so far measured for either HMXBs or LMXBs.

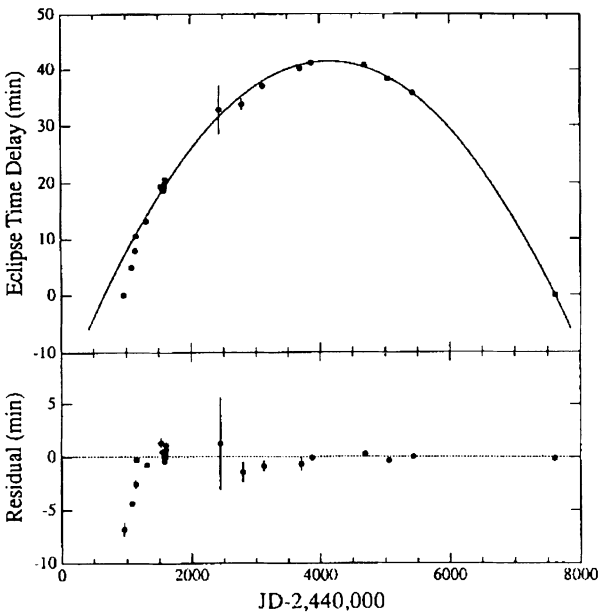

Figure 1. Delays of mid-eclipse time of Cen X-3. *Upper panel*: the observed-minus-calculated eclipse times are plotted with respect to a linear ephemeris. *Lower panel*: residuals of the observed eclipse times from the best-fitting quadratic ephemeris. (Adopted from Nagase *et al.* 1992).

Levine *et al.* (1993) analyzed the SMC X-1 data obtained with GINGA in 1987 and 1988, and found a decay of the orbit with $\dot{P}_{\rm orb}/P_{\rm orb} = (-3.36 \pm 0.02)\ 10^{-6}\,{\rm yr}^{-1}$, by combining the GINGA results with previously measured ephemerides. This rate of orbital period change is a factor of two larger than that of Cen X-3. These two binaries posses quite similar features in many respects. Based on the result, Levine *et al.* have discussed the relations between the time scales for stellar evolution, orbital decay and neutron star spin up in the SMC X-1 system.

Levine *et al.* (1991) also analyzed the GINGA data of LMC X-4, a system similar to Cen X-3. They obtained $\dot{P}_{\rm orb}/P_{\rm orb} = (1.1 \pm 0.8)\ 10^{-6}\,{\rm yr}^{-1}$ by combining their results with previously measured ephemerides, which gives a 2σ confidence range for $\dot{P}_{\rm orb}/P_{\rm orb}$ of $-0.5\ 10^{-6}\,{\rm yr}^{-1}$ to $+2.7\ 10^{-6}\,{\rm yr}^{-1}$. Combining the GINGA results with previous ephemeris measurements, Corbet *et al.* (1993) derived a rate $\dot{P}_{\rm orb}/P_{\rm orb} = (3.3 \pm 4.0)\ 10^{-6}\,{\rm yr}^{-1}$ for 4U 1538–52, suggesting a 2σ upper limit of $8\ 10^{-6}\,{\rm yr}^{-1}$. Similarly, Nagase (1992) derived a rate $\dot{P}_{\rm orb}/P_{\rm orb} = (-0.1 \pm 2.1)\ 10^{-6}\,{\rm yr}^{-1}$ for Vela X-1, yielding a 2σ upper limit of $4\ 10^{-6}\,{\rm yr}^{-1}$.

Cyg X-3 shows a clear and stable intensity modulation with a 4.8 hr period, which is generally believed to be the orbital period of the binary sys-

https://doi.org/10.1017/S0074180900055753 Published online by Cambridge University Press

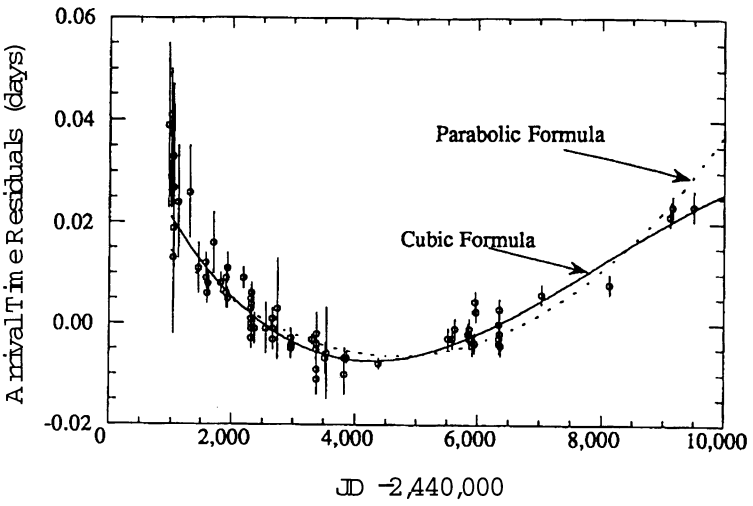

Figure 2. Arrival time residuals of the orbital modulation of Cyg X-3 with respect to a best-fit linear ephemeris. (Adopted from Kitamoto *et al.* 1995).

tem. This orbital period is typical for LMXBs. However, if the companion star is a massive Wolf-Rayet star (Van Kerkwijk *et al.* 1992; Van Kerkwijk 1993), this would be an extraordinary close system among HMXBs. An increase of the 4.8 hr period (i.e., orbital growth) was suggested by Van der Klis & Bonnet-Bidaud (1981) and this was further established by follow-up work (e.g., Kitamoto *et al.* 1987, 1992; Van der Klis & Bonnet-Bidaud 1989). Van der Klis & Bonnet-Bidaud (1989) evaluated the second derivative term $\ddot{P}_{\rm orb} = (-1.6 \pm 0.4)\ 10^{-10}\,{\rm yr}^{-1}$ from a cubic fit, implying a large decrease in $\dot{P}_{\rm orb}$, and hence $\dot{P}_{\rm orb}$ is expected to turn negative at $\sim$ 1987. New ephemerides were obtained recently from ASCA observations, and it was found that the fit to the arrival time data including these ASCA points yields significantly smaller values of $\ddot{P}_{\rm orb}$, and even a parabolic ephemeris cannot be rejected (see Fig. 2 for a comparison of the parabolic fit and the cubic fit). The global rate of period change fit to all available data for Cyg X-3 is $\dot{P}_{\rm orb}/P_{\rm orb} = (1.17 \pm 0.44)\ 10^{-6}\,{\rm yr}^{-1}$ (Kitamoto *et al.* 1995).

In addition to the above, changes of the orbital period have been reported for three LMXBs, 4U 1820–30, X 1822–371 and EXO 0748–676. Combining the latest ROSAT observations of 4U 1820–30 in 1993, Van der Klis *et al.* (1993) derived an orbital period decrease of $\dot{P}_{\rm orb}/P_{\rm orb} = (-5.3 \pm 1.1)\ 10^{-8}\,{\rm yr}^{-1}$. In contrast, an orbital period increase in X 1822–371 of $\dot{P}_{\rm orb}/P_{\rm orb} = (3.7 \pm 1.6)\ 10^{-8}\,{\rm yr}^{-1}$was reported by Hellier *et al.* (1990). EXO 0748–676 is a unique eclipsing LMXB which was discovered with EXOSAT and exhibits frequent bursts and dips. The history of the study

of orbital period change in this LMXB is also interesting. Parmar *et al.* (1991) first reported an orbital decay at a rate $\dot{P}_{\rm orb}/P_{\rm orb} \sim -2\ 10^{-7}\,{\rm yr}^{-1}$ by using the EXOSAT and the first GINGA observation. Thereafter, adopting the second and third GINGA observations, Asai *et al.* (1993) suggested that the secular tendency is rather an orbital growth at a rate $\dot{P}_{\rm orb}/P_{\rm orb} \sim 0.9\ 10^{-7}\,{\rm yr}^{-1}$. They also suggested that an ephemeris varying with a sinusoidal function provide a better fit to all the EXOSAT and GINGA data. Corbet *et al.* (1994) further confirmed this sinusoidal ephemeris by adopting recent ASCA observations, and suggested the possibility that this system is a hierarchical triplet.

TABLE 1. Measurements of Orbital Period Changes

Source Name	$P_{\rm orb}$ (days)	$\dot{P}_{\rm orb}/P_{\rm orb}$ ($\rm yr^{-1}$)	$M_{\rm opt}$ ($\rm M_\odot$)	References
Cen X-3	2.09	$(-1.738 \pm 0.004)\ 10^{-6}$	20 ± 4	1, 2, 3
SMC X-1	3.89	$(-3.36 \pm 0.02)\ 10^{-6}$	17 ± 4	4
LMC X-4	1.41	$(1.1 \pm 0.8)\ 10^{-6}$	15 ± 4	5
		$(-0.5\ 10^{-6} \leq \dot{P}_{\rm orb}/P_{\rm orb} \leq +2.7\ 10^{-6})$		
Vela X-1	8.96	$(-0.1 \pm 2.1)\ 10^{-6}$	23 ± 2	6
		$(\lvert \dot{P}_{\rm orb}/P_{\rm orb} \rvert \leq 4\ 10^{-6})$		
4U 1538–52	3.73	$(3.3 \pm 4.0)\ 10^{-6}$	20 ± 4	7
		$(\lvert \dot{P}_{\rm orb}/P_{\rm orb} \rvert \leq 8\ 10^{-6})$		
Cyg X-3	0.02	$(1.17 \pm 0.44)\ 10^{-6}$	(~ 10)	8, 9, 10
Her X-1	1.70	$(-1.32 \pm 0.16)\ 10^{-8}$	2.0 ± 0.2	11
4U 1820–30	0.008	$(-5.3 \pm 1.1)\ 10^{-8}$	($\sim$0.06)	12
4U 1822–371	0.23	$(3.7 \pm 1.6)\ 10^{-7}$	($\sim$0.3)	13
EXO 0748–67	0.16	(sinusoidal variation?)	($\sim$0.2)	14, 15, 16

References: 1; Murakami *et al.* 1983, 2; Kelley *et al.* 1983, 3; Nagase *et al.* 1992, 4; Levine *et al.* 1993, 5; Levine *et al.* 1991, 6; Nagase 1992, 7; Corbet *et al.* 1993, 8; Kitamoto *et al.* 1987, 9; van der Klis and Bonnet-Bidaud 1989, 10; Kitamoto *et al.* 1995, 11; Deeter *et al.* 1991, 12; van der Klis *et al.* 1993, 13; Hellier *et al.* 1990, 14; Parmar *et al.* 1991, 15; Asai *et al.* 1992, 16; Corbet *et al.* 1994.

The derived rates of orbital period change are summarized in Table 1, together with the orbital periods and estimates of the companion masses. The rates are also plotted in Fig. 3 against the estimated companion mass. For X-ray pulsar systems, the masses of the companion star are calculated from measurements of the orbital Doppler delay curve of the X-ray sources (neutron stars) and of the optical radial-velocity curve of the companion stars. Values are adopted from Nagase (1989), except for 4U 1538–52 for which an improved value is adopted from recent measurements of the

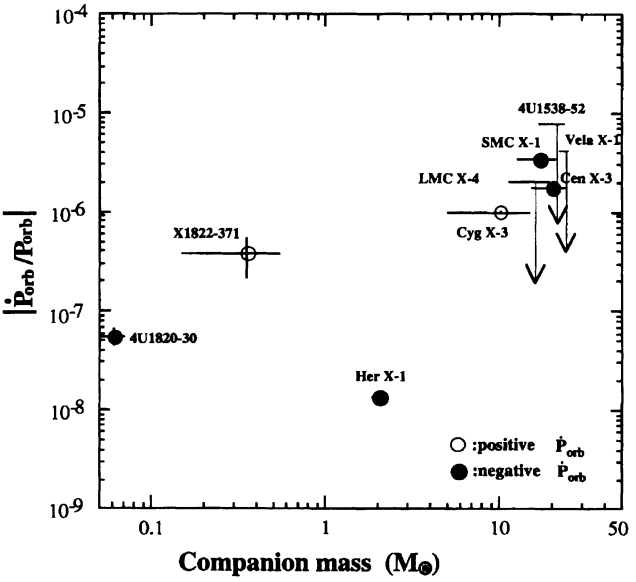

Figure 3. The magnitudes of the rate of change of the orbital period in X-ray binaries plotted against the mass of companion stars.

companion radial-velocity curve (Reynolds *et al.* 1992). For others sources, nominal masses estimated for the particular classes of companion stars are cited.

Although there are several mechanisms that cause the orbital period to change (see e.g., Bhattacharya & Van den Heuvel 1991), gravitational radiation loss from the binary system and mass transfer from a massive donor star to the neutron star cannot extract enough angular momentum from the system to explain the orbital decays measured in these massive binary pulsars. If the massive companion is not co-rotating with the orbit, tidal friction due to asynchronism becomes an effective mechanism of orbital period change (Kelley *et al.* 1983). Both orbital decay and growth are possible by this model depending on the ratio of the rotation frequency of the companion star and the orbital frequency. Levine *et al.* (1991, 1993) have interpreted the observed rate of change in Cen X-3, SMC X-1 and LMC X-4 all consistently with this scheme. They further suggest that Her X-1 is located in the regime of stable tidal equilibrium (i.e., synchronous rotation).

Since a naive mass transfer model does not explain the observed rate of orbital period change in Her X-1, Deeter *et al.* (1991) adopted a model of magnetically channeled flow. If Her X-1 possesses a wind with mass flow rate comparable to the mass accretion rate, and the companion star has a magnetic field of several tens of Gauss at the stellar surface, then the

material is channeled to a large distance of the Alfvén radius and the torque exerted by the material explains the observed rate of change in Her X-1.

Mass loss via a stellar wind could be a plausible mechanism for causing an observable rate of change in the orbital period, if the mass loss rate of the companion star is large. This mechanism may explain the observed orbital growth in Cyg X-3, since the mass loss rates of Wolf-Rayet stars are generally large (Van Kerkwijk *et al.* 1992). From the observed rate of change in orbital period, a mass loss rate $\dot{M}_{\rm w} = \dot{P}_{\rm orb} M / 2P_{\rm orb} \sim 6\ 10^{-6}\,{\rm M}_\odot\,{\rm yr}^{-1}$ is derived, assuming the companion star mass to be $10\,{\rm M}_\odot$ (Kitamoto *et al.* 1995). Thus, the interpretation of angular momentum loss via a stellar wind is plausible, since the estimated mass loss rate is in the typical range for Wolf-Rayet stars.

3. X-Ray Spectroscopy of HMXBs with ASCA

About a dozen typical HMXBs were observed during the initial 6 month performance verification phase of ASCA. High resolution X-ray spectra were obtained from these observations using the SIS detectors (CCD cameras). Spectroscopic results obtained from Vela X-1, Cen X-3 and Cyg X-3 are presented and discussed in this section.

Typical HMXBs have an evolved early-type companion star with a strong stellar wind. A neutron star orbiting the massive primary star captures the wind and X-ray emission is produced in the vicinity of the neutron star. The X-ray photons irradiate and ionize the surrounding wind, thus forming a photo-ionized sphere surrounding the neutron star. Since the direct beam from the neutron star is blocked by the companion star during eclipse phases, reprocessed X-ray emission from the photo-ionized stellar wind can be observed without contamination by the stronger direct beam. At the phase after ingress of the neutron star we can probe the trailing side of the photo-ionized sphere, then the outer region at the mid-eclipse phase, and finally the leading side of the sphere before egress from eclipse. Thus, the summed eclipse spectrum yields X-ray emission from the whole photo-ionized region.

3.1. VELA X-1

Vela X-1 is an eclipsing wind-fed X-ray binary pulsar. It is a relatively wide system with an 8.96 d orbital period, an eclipse duration of 1.7 d, and a long pulse period of 283 s. This pulsar was observed with ASCA in June and July 1993, covering an entire eclipse transition by the two observations. The spectrum obtained during an eclipse phase, when the direct beam from the vicinity of the neutron star disappears, is shown in Fig. 4.

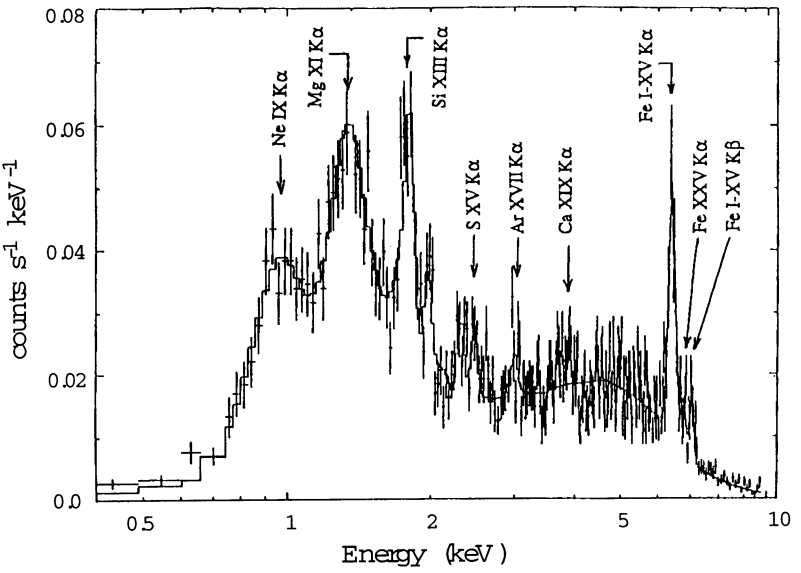

Figure 4. Energy spectrum of Vela X-1 obtained with the SIS0 detector (CCD camera) on board ASCA during the eclipse phase. A model spectrum convolved from the best-fit parameters is compared to the data by a histogram.

Remarkably, the spectrum consists of many intense lines from 0.9 keV to 7 keV that are superposed on the flat continuum. The energies of these lines and their tentative identifications are indicated in the figure. In addition to the iron Kα line at 6.4 keV and the Kβ line at 7.05 keV, which are reprocessed by iron in low-ionization states, one can see Kα lines from highly ionized He-like ions of Ne, Mg, Si, S, Ar, Ca and Fe. Although the lines at 0.9 keV and 1.3 keV are apparently wide, these widths may be not intrinsic, but due to blending of H-like Kα lines of Mg and Si, and of L-shell transition lines of Fe with the He-like Kα lines. This spectral feature suggests that the stellar wind surrounding the neutron star is a multi-zone structure with different degrees of ionization.

The features dominated by the He-like lines are interpreted as the radiative recombination Kα lines followed by cascades (Hatchett *et al.* 1976). As calculated by McCray *et al.* (1984), the stellar wind near the neutron star can be easily ionized to high ionization stages by irradiation of hard X-rays from the neutron star. Thus, zones of different ionization are formed surrounding the neutron star. Contrary to the thermal-equilibrium plasma, the electron temperature of this photo-ionization plasma is relatively low, typically about 100 eV (Kallman & McCray 1982). Thus radiative recombination followed by cascades becomes a dominant process. If this is the case, the line-like emission above the recombination edge due to the free-bound

transitions should also be considerable. By coincidence, the edge energies of He-like and H-like oxygen lie near the Kα line of He-like Ne, and the edges of Ne lie around the Mg line, etc. It is difficult, unfortunately, to resolve these edge emission structures and the transition lines in the present spectrum because of the limited resolution and statistics.

3.2. CENTAURUS X-3

Cen X-3 is another typical eclipsing X-ray binary pulsar with an orbital period of 2.09 d, an eclipse duration of 0.4 d and a pulse period of 4.84 s^{-1}. This pulsar is very luminous and the companion is an O-type star, hence it is believed that an accretion disk and stellar wind co-exist in this system. This X-ray pulsar Cen X-3 was observed with ASCA in June 1993, throughout an entire eclipse transition from a pre-eclipse dip phase to eclipse egress.

Kα emission lines of the H-like ions of Mg and Si are visible in the spectra obtained both during the pre-eclipse and mid-eclipse phases of Cen X-3, in addition to the iron emission lines. This is in contrast with the Vela X-1 eclipse spectrum, in which Kα lines from He-like ions dominate. This may be caused by the fact that the luminosity of Cen X-3 is more than an order of magnitude larger than that of Vela X-1; therefore, the ionization of the surrounding stellar wind in this system will be more complete as calculated by Hatchett & McCray (1977).

Three emission lines of Fe can be resolved at 6.4, 6.7 and 6.9 keV, in addition to an absorption edge at 7.1 keV in both the pre-eclipse and mid-eclipse spectra (Ebisawa *et al.* 1995). As seen in Fig. 5, the intensity of the 6.4 keV fluorescent line is prominent at the pre-eclipse phase but is extremely reduced during the eclipse phase. However, the intensities of the 6.7 keV line due to He-like ions of Fe and the 6.9 keV line due to H-like ions of Fe remain about the same in the two phases. These results suggest that the fluorescent 6.4 keV line is produced by cold matter located relatively close to the neutron star, whereas the 6.7 keV and 6.9 keV lines are attributed to the hot highly ionized plasma spread out over the size of companion star. Similar results were suggested previously by Nagase *et al.* (1992) by analyzing the GINGA data. However, in their analysis they assumed *a priori* two narrow lines at 6.4 keV and 6.7 keV and derived the intensities of the two lines from the shift of the center energy in the observed line, which is apparently broad due to the poor resolution of the GINGA proportional counters. In contrast the ASCA observations resolve all three lines.

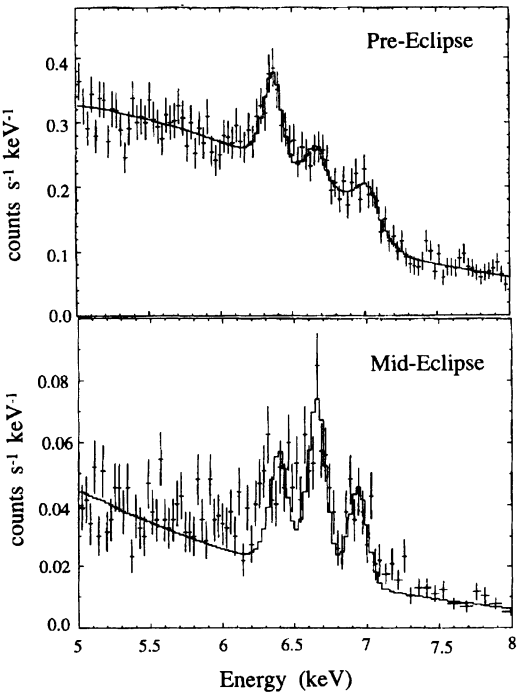

Figure 5. Energy spectra of Cen X-3 in the range of 5-8 keV obtained with the ASCA SIS0 detector. The three iron lines resolved at 6.4 keV, 6.7 keV and 6.9 keV are compared to the spectrum obtained during pre-eclipse phase and that obtained during mid-eclipse phase. Model spectra convolved from the best-fit parameters are compared to the data by a histogram.

3.3. CYGNUS X-3

Cyg X-3 was observed with ASCA during the PV phase on June 11, 1993 in its high-intensity state. The spectrum obtained by the CCD camera is shown in Fig. 6, averaged over the 4.8 hr orbital period. Using this ASCA spectrum Kitamoto *et al.* (1994) resolved for the first time the broad Fe emission line into three components at 6.4 keV, 6.7 keV and 6.9 keV They also found that the 6.7 keV and 6.9 keV lines are modulated with the 4.8 hr orbital period with a phase lag relative to the continuum; the line intensities are at maximum when the continuum intensity is at minimum.

In addition, Kα lines of both the He-like and H-like ions of Si, S, Ar, and Ca are clearly visible in the spectrum (see Fig. 6). The prominent H-like Kα lines of Si and S do not show the 4.8 hr orbital modulation unlike the

https://doi.org/10.1017/S0074180900055753 Published online by Cambridge University Press

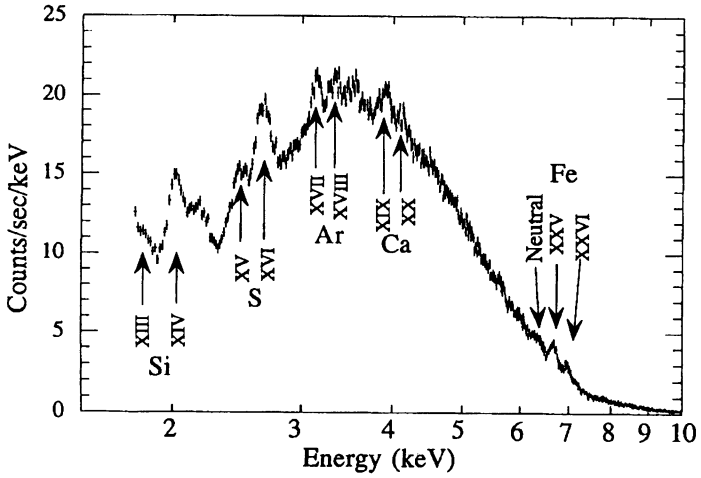

Figure 6. Energy spectrum of Cyg X-3 obtained with the ASCA SIS0 detector. Identifications of prominent lines are indicated by arrows. (Adopted from Kitamoto *et al.* 1994).

iron line. Those lines from lighter elements cannot originate from the same region that emits the He-like and H-like Kα lines of iron. Nevertheless, the plasma is in thermal equilibrium or in photo-ionization equilibrium, the spectrum can hardly be fitted by a simple plasma model. These emission lines and their orbital phase dependences may provide crucial clues to the understanding of the X-ray emission from the enigmatic X-ray binary Cyg X-3.

Acknowledgements. The author would like to express his thanks to all the ASCA team members. Particular thanks are due to Drs. S. Kitamoto and K. Ebisawa for providing data prior to publication. He is also grateful to Dr. S. Skinner for his careful review of the manuscript.

References

Asai, K. *et al.* 1992, PASJ 44, 633
Bhattacharya, D. & Van den Heuvel, E.P.J. 1991, Phys. Rep. 203, 1
Corbet, R.H.D., Woo, J.W. & Nagase, F. 1993, A&A 276, 52
Corbet, R.H.D. *et al.* 1994, ApJ 436, L15
Deeter, J.E. *et al.* 1991, ApJ 383, 324
Ebisawa, K. *et al.* 1995, (in preparation)
Hatchett, S. & McCray, R. 1977, ApJ 211, 552
Hatchett, S., Buff, J. & McCray, R. 1976, ApJ 206, 847
Hellier, C. *et al.* 1990, MNRAS 244, 39P
Kallman, T.R. & McCray, R. 1982, ApJS 50, 263

Kelley, R.L. *et al.* 1983, ApJ 268, 790
Kitamoto, S. *et al.* 1987, PASJ 39, 259
Kitamoto, S. *et al.* 1992, ApJ 384, 263
Kitamoto, S. *et al.* 1994, PASJ 46, L105
Kitamoto, S. *et al.* 1995, (in preparation)
Levine, A. *et al.* 1991, ApJ 381, 101
Levine, A. *et al.* 1993, ApJ 410, 328
McCray, R. *et al.* 1984, ApJ 282, 245
Murakami, T. *et al.* 1983, ApJ 264, 563
Nagase, F. 1989, PASJ 41, 1
Nagase, F. 1992, in *Frontiers of X-Ray Astronomy*, Y. Tanaka & K. Koyama (Eds.), Uni. Acad. Press, Inc., Japan, p. 79
Nagase, F. *et al.* 1992, ApJ 396, 147
Nagase, F. *et al.* 1994, ApJ 436, L1
Parmar, A.N. *et al.* 1991, ApJ 366, 253
Reynolds, A.P., Bell, S.A. & Hilditch, R.W. 1992, MNRAS 256, 631
Van der Klis, M. & Bonnet-Bidaud, J.M. 1981, A&A 95, L5
Van der Klis, M. & Bonnet-Bidaud, J.M. 1989, A&A 214, 203
Van der Klis, M. *et al.* 1993, A&A 279, L21
Van Kerkwijk, M.H. 1993, A&A 276, L9
Van Kerkwijk, M.H. *et al.* 1992, Nat 355, 703

Discussion

R.A.M.J. Wijers: What is the accuracy with which the positions of emission line centers can be determined using ASCA? Is there any hope of measuring velocities of the line forming region?

F. Nagase: The nominal accuracy is 20 eV for the position of a line center. The instrumental energy resolution is 120 eV at 6 keV.

Note to answer by R. Wijers: This means one can measure a velocity of $\frac{v}{c} \simeq \frac{20\,\mathrm{eV}}{5\,\mathrm{keV}} = 4\,10^{-3}$, i.e. $v \simeq 1200\,\mathrm{km\,s^{-1}}$. This is probably not small enough to measure orbital velocities in realistic cases, except perhaps if one uses 10 lines in one source and the line forming process is well-understood and simple (then $\triangle \mathrm{E} \sim 20\,\mathrm{eV}/\sqrt{10} \sim 6\,\mathrm{eV}$, and $v \sim 350\,\mathrm{km\,s^{-1}}$. An example of this procedure is the work done with ASCA on SS433.